Dynamic Supramolecular Chemistry | Hot Paper

How to cite: *Angew. Chem. Int. Ed.* **2021**, *60*, 2855–2860
International Edition: doi.org/10.1002/anie.202011740
German Edition: doi.org/10.1002/ange.202011740

Real-Time Visual Monitoring of Kinetically Controlled Self-Assembly

Zizhao Huang, Tao Jiang, Jie Wang, Xiang Ma, and He Tian*

Abstract: *The construction of artificial structures through hierarchical self-assembly based on noncovalent interactions, as well as monitoring during the self-assembly process, are important aspects of dynamic supramolecular chemistry. Herein we describe the complex dynamics of chiral N,N′-diphenyl dihydrodibenzo[a,c]phenazine derivatives (S)/(R)-**DPAC**, whose different assemblies were found to have distinct optical and morphological characteristics. With ratiometric fluorescence originating from vibration-induced emission (VIE), the self-assembly process from kinetic traps to the thermodynamic equilibrium state could be monitored in real time by optical spectrometry. During the morphology transformation from particles to nanobricks, strong circularly polarized luminescence was induced with $g_{lum} = 1.6 \times 10^{-2}$. The excited-state characteristics of the self-assemblies enabled investigation of the relationship between molecular aggregation and conformational change, thus allowing effective monitoring of the sophisticated supramolecular self-assembly process.*

It has been proved that small molecules can self-assemble into various nano- or microscopic structures hierarchically via noncovalent interactions, paving a significant way to materials chemistry.[1] Traditionally, the construction of self-assembly was considered as thermodynamic equilibrium structures, but investigations on the kinetic pathways of product formation were largely neglected. Intrinsically, supramolecular self-assembly tends to be "dynamic" in nature ascribed to the reversible noncovalent interactions. Thus, the dynamic nature opens up interesting possibilities for application and further exploration, including dynamic optical materials,[2] self-healing materials[3] and self-replicating systems.[4] Among them, a rising number of novel studies are cast into the field of kinetically controlled self-assembly pathways base on dynamic process.[5] A precise understanding of self-assembly processes can give greater control over size and architecture of the supramolecular aggregates.[6] But the means to monitor the process during self-assembly of dynamic supramolecules still remains to be developed. Traditionally, these processes are studied by such techniques as electron microscopy and nuclear magnetic resonance spectroscopy.[7] Sample pretreatment before instrumental detection and following analysis were carried out under harsh conditions. Although great efforts have been devoted, a simple method to investigate the molecular aggregation and conformational change remains a formidable challenge. Since the excited state of chromophores exhibits sensitivity to conformation, orientation and supramolecular state, optical spectrometry is an excellent candidate for investigating the transitional process of self-assembly. However, the realization of the visual monitoring of the self-assembly process by utilizing distinct luminescence behavior was rarely reported.

A recent study from Tian's group indicates that a class of novel fluorogens show the unique vibration-induced emission (VIE) effect. The molecules in solution undergo an excited-state configuration transformations from a bent shape (intrinsic state) to a planar shape (planarized state), inducing the effective π-conjugation thus emitting red fluorescence. While in the solid or aggregation state, the physical constraint blocked the planarization of the structure in the excited state, result in an emission of intrinsic blue light.[8] The research sparked the inspiration to explore the possibility of applying VIE molecules to in situ and real-time detection of the self-assembling construction. Different aggregations enabled distinctly oriented and ordered structures of individual molecules during self-assembly. The noncovalent bond driven self-assembly was expected to be employed to regulate the excited-state deformation of VIE molecules as a structural element in the preparation of dynamic process, and then the process can be effectively monitored using spectroscopy. In addition, chirality in molecular units and assemblies is a state that are derived from the dissymmetry of the environment, and the fascinating chiroptical properties exhibited by such systems are frequently employed to investigate the relationship between molecular aggregation and conformational change.[9] Therefore, with distinct dual fluorescence emissions, large Stokes shift and prominent chiral luminescence, the unique behaviors of chiral VIE are likely to be applied in the detection of molecular self-assembly process efficiently.

Herein, we described the synthesis and self-assembly features of chiral VIE derivatives (*S*)/(*R*)-**DPAC**, which are composed of chiral cyclohexanediamine and two *N*,*N*′-diphenyl dihydrodibenzo[*a*,*c*]phenazine moieties (Figure 1 a). In the solution of THF/H_2O = 3/7 (v/v), the chiral derivatives deformed into kinetically favored metastable assembly with red fluorescent forms quickly but then spontaneously transformed into the blue fluorescent thermodynamically favored form. With the synergistic combination of supramolecular and photochemical strategies, the complex self-assembly pathway was investigated fully. More significantly, due to the chiral center in the molecule, accompanying with the morphology transformation from particles to chiral nanobricks, the nano-

[*] Z. Huang, Dr. T. Jiang, J. Wang, Prof. X. Ma, Prof. H. Tian
Key Laboratory for Advanced Materials and
Feringa Nobel Prize Scientist Joint Research Center
Frontiers Science Center for Materiobiology and Dynamic Chemistry
School of Chemistry and Molecular Engineering
East China University of Science and Technology
Meilong Road 130, Shanghai 200237 (P. R. China)
E-mail: maxiang@ecust.edu.cn
Supporting information and the ORCID identification number(s) for the author(s) of this article can be found under: https://doi.org/10.1002/anie.202011740.

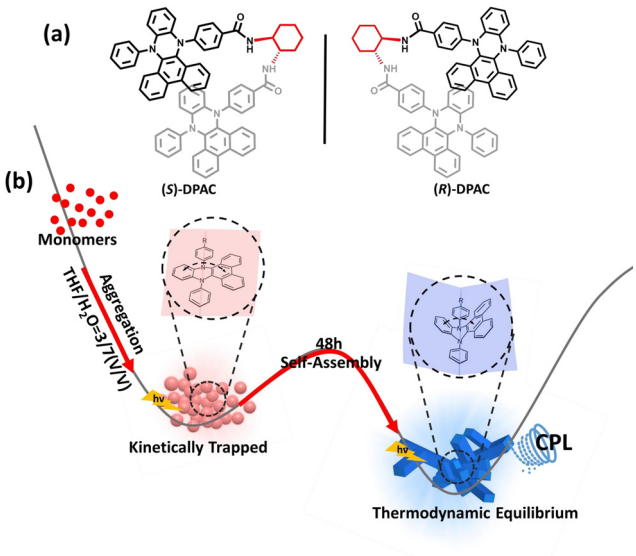

Figure 1. a) Structures of chiral molecules (*S*)/(*R*)-**DPAC**. b) Illustration of the morphological transition.

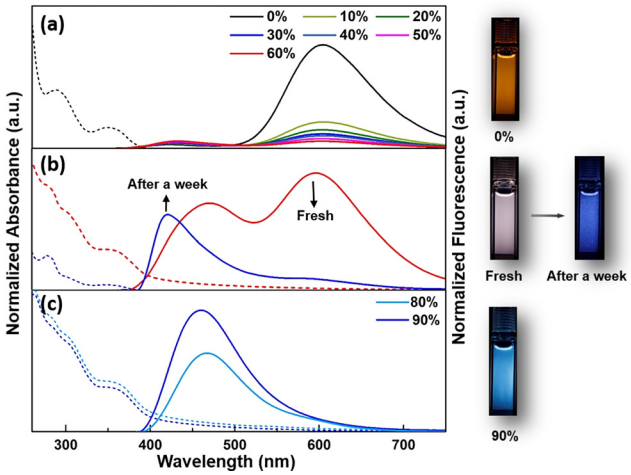

Figure 2. Normalized absorbance (dashed lines) and fluorescence spectra (solid lines) of (*R*)-**DPAC** in THF/H_2O (v/v) solvents with a water fraction of a) 0–60%, b) 70%, and c) 80–90% at 298 K, and corresponding photographs taken under 365 nm UV light. ([(*R*)-**DPAC**] = 1×10^{-5} M, λ_{ex} = 350 nm).

bricks can induce strong circularly polarized luminescence (CPL) with $g_{lum} = 1.6\times10^{-2}$.

Compounds (*S*)/(*R*)-**DPAC** were prepared according to the synthetic route presented in Figure S1. ^{1}H NMR, ^{13}C NMR and electronic spray ionization (ESI) high-solution mass spectroscopy analyses were employed to confirm their structures (detailed characterization data see Supporting Information, Figure S2–S7). (*R*)-**DPAC** was picked out as the representative for the following elaboration. The details of enantiomer (*S*)-**DPAC** were presented in the supporting information.

The photophysical properties were investigated by UV/Vis absorption and fluorescence spectroscopy. (*R*)-**DPAC** exhibited typical VIE properties, which presented different emissive behaviors in solid state and solution (Figure S9). The long-wavelength emissions from the solution state located at 610 nm, while the short-wavelength emission from the solid state at 485 nm. The distinct emission was ascribed to unique excited-state configurations. Analogously, the phenomenon could be achieved in different ratio of THF/H_2O (v/v) mixtures through affecting the aggregation state (Figure 2, S10). As the fraction of water (f_w) increased from 0% to 60%, the red emission of (*R*)-**DPAC** was quenched gradually due to the intramolecular charge transfer caused by the increasing solvent polarity. When the water fraction increased to 80% or 90%, the (*R*)-**DPAC** molecules aggregated and then the planarization process of the excited-state induced by vibration was suppressed and the blue emission located at 450 nm was observed. Intriguingly, in the water fraction of 70%, both red and blue emission intensity increased obviously. Besides, the freshly prepared mixtures in this condition were turbid but became clear due to the sedimentation of aggregates after one week, along with the emission color changing from pink to blue. However, such unstable state was not found in other water fraction and not influenced by concentration (Figure S11, S12). After standing, (*R*)-**DPAC** was re-concentrated to perform structural confirmation and fluorescence spectra, suggesting that the phenomenon was not originated from degradation and exhibited reproducibility properties (Figures S8 and S13).

To further investigate the process, we then conducted the in situ and time-dependent spectra to monitor the transformation in the above critical systems (f_w = 70%). As shown in the time-dependent fluorescence spectra (Figure 3a), the fluorescence curve of the freshly prepared (*R*)-**DPAC** solution showed a blue emission located at 470 nm and relatively strong red emission at 595 nm, respectively. A sharp decrease in the fluorescence intensity was observed within the next 6 h, whereafter a new emission appeared at 425 nm and the intensity gradually increased over the subsequent period, while the red fluorescence at 595 nm was completely faded away finally. The corresponding CIE coordinate diagram clearly shows the change of luminescence during the process (Figure 3b). In time-dependent absorption spectra, the absorption of (*R*)-**DPAC** showed a slight bathochromic shift and broadening gradually as time goes, which indicated the formation of aggregates (Figure S15). According to the characteristics of VIE,[8a] this distinct emission was ascribed to unique excited-state configurations of different molecular assembly states. Therefore, we speculated that it possibly exists a complex system in which different aggregation pathways lead to the formation of distinct assemblies. In a more rigid assembly, the planarization process of the excited-state induced by vibration was suppressed, showing a smaller degree of bending angle, resulting in an emission of intrinsic blue light.

Hence, we carried out X-ray diffraction (XRD) to clarify the formation of aggregates. The diffraction pattern of (*R*)-**DPAC** exhibited only one broad peak which indicated the formation of amorphous structures. For samples left standing for one week, new diffraction peaks were observed, indicating the molecules have ordered molecular packing and crystalline nature to some extent (Figure S16). Besides, the process of change was extremely slow. It could be reasonably envisaged

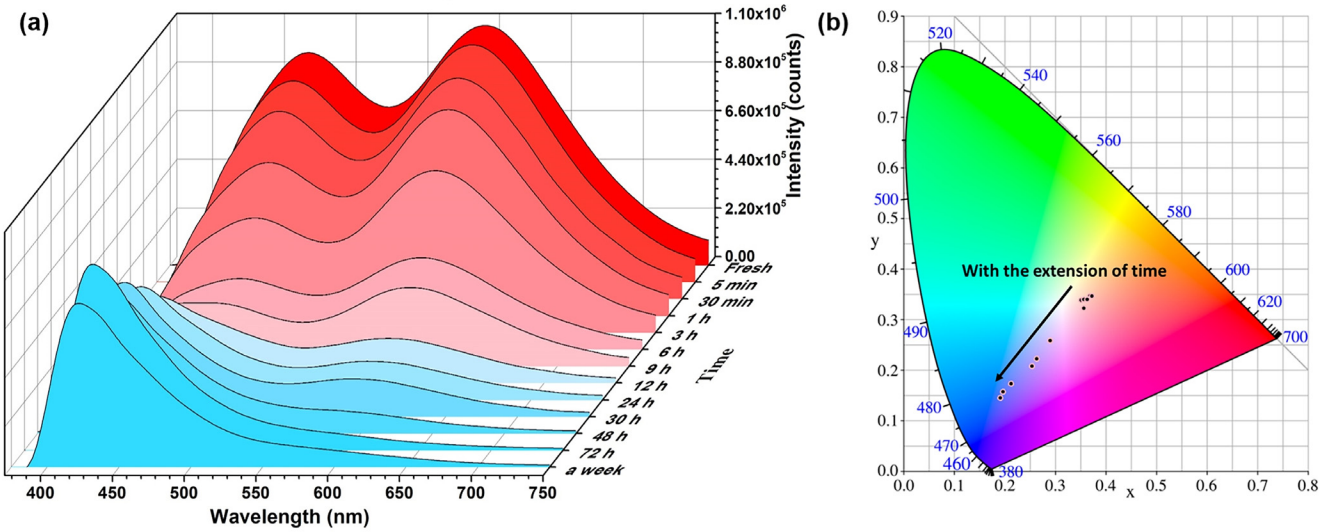

Figure 3. a) Time-dependent fluorescence spectra of (*R*)-**DPAC** in THF/H_2O (3/7, v/v) mixtures at 298 K. ([(*R*)-**DPAC**] = 1×10^{-5} M, λ_{ex} = 350 nm). b) Corresponding 1931 CIE coordinate diagram of (*R*)-**DPAC** with different times.

that the reason for this change was the multiple coefficient factors in the condition of $f_w = 70\,\%$, the (*R*)-**DPAC** entered a thermodynamic non-equilibrium state (i.e., kinetically trapped aggregates), ripened to form another morphology over time, which resulted in the blocked configuration transformations of the VIE molecules in the excited state, thus influence the emission finally.

Complex self-assembly pathway originates from a combination of different noncovalent force that govern inter/intramolecular interactions and spontaneous aggregation, where out-of-equilibrium states can appear under specific conditions.[10] Compounds (*R*)/(*S*)-**DPAC** possesses a π-conjugated structure in favor of the intermolecular π–π stacking interactions, which are predicted to induce and direct self-assembly under certain conditions. Besides, it contains a cyclohexane–dicarboxamide moiety capable of engaging a directional hydrogen bond, such as N–H. These different groups played a critical role in the self-assembly because multiple interactions provide the contributions in solvents with different polarities.[11] Hence, a volume ratio of THF/H_2O of 3/7 was critical for the transition and formation of the observed self-assembly, which provides suitable driving force for the formation of nanostructure self-assembly.

From the perspective of morphology characterization to confirm our hypothesis, the transitional process of self-assembly (the morphological transformation at different ripening time) was investigated by dynamic light scattering (DLS), scanning electron microscope (SEM) and atomic force microscope (AFM). Due to the extremely slow assembling process, we selected several representative times (fresh, 3 h, 9 h, 24 h, 48 h) as the experimented samples. Together with results from DLS, SEM and AFM studies (Figure 4, S17, S18), in the condition of $f_w = 70\,\%$, the nanoparticles with a relatively narrow size distribution at around 830 nm was the largest compared with other ratios. It suggested that the fresh prepared (*R*)-**DPAC** would tend to aggregate together to minimize the surface energy with the formation of soft nanoparticles. The phenomenon indicates that the different aggregation modes of assemblies enables them to experience a kinetically trapped state. According to size and spherical shape confirmed by SEM analysis, we presumed that the directional hydrogen bond donor amido group formed the interior and exterior coronas, while the π-conjugated VIE group probably became the membrane of the particle. The molecules can undergo an excited-state configuration transformation because the particles with a disorder arrangement have a certain flexibility at this time, thus generating dual emission, which was consistent with the luminescence spectra, whereafter the particles began to coalesce one by one and formed a bricklike morphology after 3 h of incubation. The nanostructures became elongated with time progress and the particles became fewer simultaneously, revealing that the gradual growth of the nanobricks. After 48 h, substantially elongated aggregates were formed, accompanied by the complete disappearance of the precursor particles. The size change during morphology transformation can also be clearly presented in time-dependent DLS. The nanobricks morphology remained unchanged for a few weeks in solution, indicating the thermodynamically stable characteristic (Figure S19). However, no significant assemblies were observed after one week in other water fractions (Figure S20). Hence, the results of the above time-dependent experiment demonstrated that, in $f_w = 70\,\%$ mixture, multiple coefficient interactions in this condition favor the formation of metastable inactivated monomers that entered a kinetically trapped state, and underwent morphological transitions in self-assembly process to a thermodynamically stable state.

Reflecting the structural information of the excited state in the chiral luminescence architecture, CPL, was employed to investigate the transitional process of self-assembly.[12] Both *S* and *R* isomers exhibited circular dichroism (CD) signals in various solvents with positive and negative first Cotton effects, respectively (Figure S21). In THF/H_2O = 3/7 (v/v) mixtures, the poor solubility of the newly formed

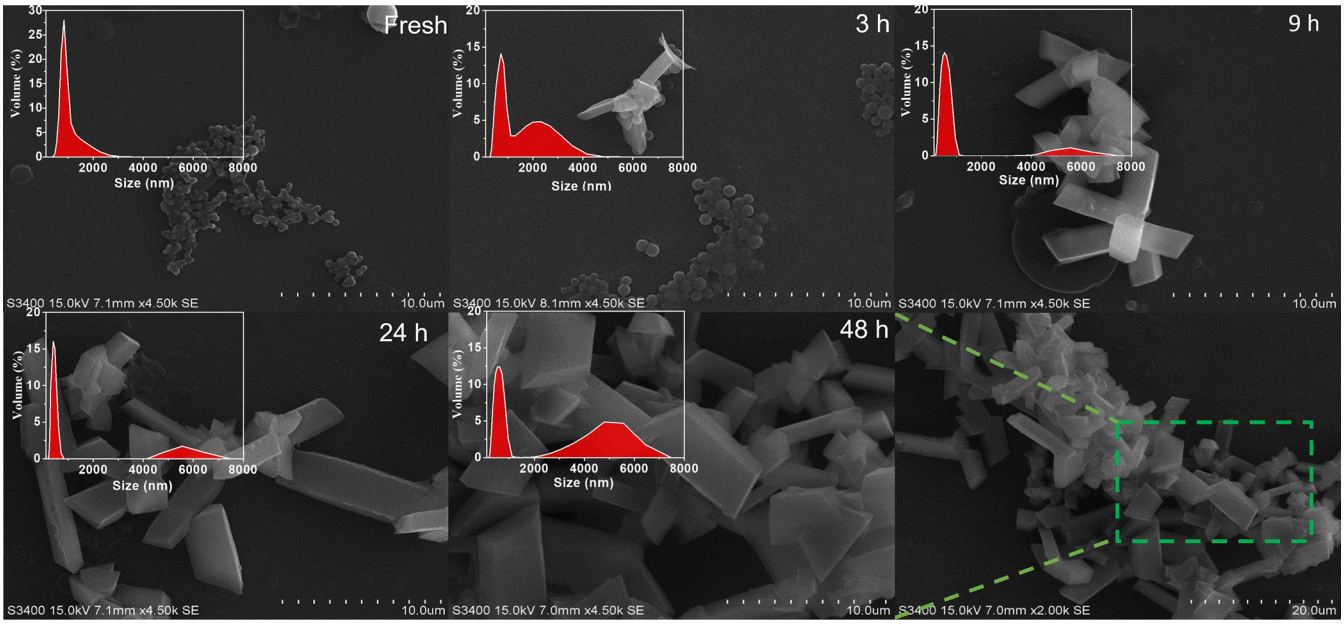

Figure 4. Time-dependent SEM images to visualize the self-assembly processes of (*R*)-**DPAC** in THF/H_2O (3/7, v/v) mixtures at 298 K. Inset: Time-dependent DLS of (*R*)-**DPAC**.

nanobricks lead to the decrease in the effective concentration of solution and thus gradually weakened CD signal (Figure 5a). Besides, since the orderly molecular stacking of nanobricks was conducive to the generation of chiral environment, the CPL intensity dramatically enhanced accompanying with the morphology transformation, which exhibited a similar tendency with fluorescence spectra at 425 nm (Figure 5b). The enhanced CPL intensity of time-dependent morphology transformation demonstrated that the CPL activity presented morphological dependence precisely. Furthermore, the CPL properties of thin films were similar with the solution (Figure S23), indicating the CPL characteristics could be applied to the solid state as well.

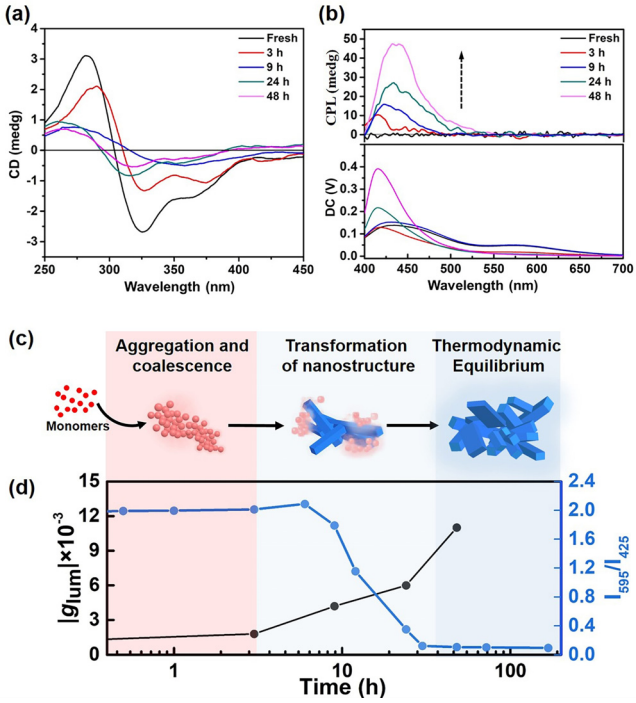

Figure 5. Time-dependent a) CD spectra and b) CPL spectra of (*R*)-**DPAC** in THF/H_2O (3/7, v/v) mixtures at 298 K. c) Illustration of the morphological transition. d) Time-dependent relative fluorescence intensity ratios of 595 nm/425 nm (blue line) and g_{lum} (black line) for (*R*)-**DPAC** in THF/H_2O (3/7, v/v) mixtures. Time is expressed logarithmically. ([(*R*)-**DPAC**] = 1×10^{-5} M.)

Due to these significant changes in emission colors during self-assembly, we realized that the fluorescence spectra could serve as a rapid and effective tool for the monitoring of the system evolution. Besides, CPL activity exhibited accurate morphological dependence, the g_{lum}, quantified the extent of chiral dissymmetry in fluorescence, can employ as another powerful technique to monitor chiral assembly in supramolecular systems simultaneously. The use of such methodologies to monitor the excited-state properties and unravel the pathway of the self-assembly processes were novel alternative compared with the more-common absorption or circular dichroism methods. As shown in Figure 5c and 5d, with the ratiometric fluorescence change originated from the VIE feature, the transformation of the nanostructure corresponds exactly with the spectrum. The distinct luminescent performance makes the monitoring of the morphological transition feasible. Besides, the g_{lum} value of the obtained sample was 2.9×10^{-3} at the first 3 h. After ripening for 48 h, the g_{lum} value reached to 1.6×10^{-2}, which was almost six times as long as 3 h. Concomitantly, the significant increase in g_{lum} was consistent with the morphology transformation. Hence, the entire supramolecular self-assembly process could be followed facilely by monitoring the apparent fluorescence color change and g_{lum} during the whole experiment.

In conclusion, we managed complex dynamics of VIE derivatives (*S*)-**DPAC** and (*R*)-**DPAC** that involve different

assemblies with distinct optical and morphological properties. When exposed the two derivatives in special environment of THF/H_2O (3/7, v/v), the critical mixture solvent can direct it into metastable aggregations with red fluorescence, which can be spontaneously transformed into thermodynamically favored blue fluorescent nanobricks. With the tunable fluorescence originated from the VIE feature, the spectral change corresponds precisely to morphological transition, offered the possibility of real-time monitoring of the self-assembly process involved. Besides, accompanying with the morphology transformation from particles to nanobricks, the ordered packing of nanostructures induced the strong circularly polarized emission, which can contribute a large g_{lum} value with 1.6×10^{-2}. Through the engineering of excited-state, the spectra offered a compendious approach to investigate the relationship between molecular aggregation and conformational change, enabling a great potential for fabricating smart optical nanomaterials.

Acknowledgements

We gratefully acknowledge financial support from the National Natural Science Foundation of China (21788102, 22020102006, 21722603 and 21871083), project support by the Shanghai Municipal Science and Technology Major Project (Grant No.2018SHZDZX03), the Program of Shanghai Academic/Technology Research Leaders (20XD1421300), the "Shu Guang" project supported by Shanghai Municipal Education Commission and Shanghai Education Development Foundation (19SG26), the Innovation Program of Shanghai Municipal Education Commission(2017 01–07-00-02-E00010), and the Fundamental Research Funds for the Central Universities. We thank Prof. Y. Cheng (Nanjing University) and Prof. L. Feng (Shanghai University) for their kind assistance. Helpful discussions with Z. Yuan, X. Jin, and L. Ma are also acknowledged.

Conflict of interest

The authors declare no conflict of interest.

Keywords: circularly polarized luminescence · kinetic traps · self-assembly · vibration-induced emission · visual monitoring

[1] a) C. Rest, R. Kandanelli, G. Fernandez, *Chem. Soc. Rev.* **2015**, *44*, 2543 – 2572; b) L. Yang, X. Tan, Z. Wang, X. Zhang, *Chem. Rev.* **2015**, *115*, 7196 – 7239; c) X. Ma, J. Wang, H. Tian, *Acc. Chem. Res.* **2019**, *52*, 738 – 748.

[2] a) X. M. Chen, Y. Chen, Q. Yu, B. H. Gu, Y. Liu, *Angew. Chem. Int. Ed.* **2018**, *57*, 12519 – 12523; *Angew. Chem.* **2018**, *130*, 12699 – 12703; b) J. Wang, Z. Huang, X. Ma, H. Tian, *Angew. Chem. Int. Ed.* **2020**, *59*, 9928 – 9933; *Angew. Chem.* **2020**, *132*, 10014 – 10019; c) T. Jiang, X. Wang, J. Wang, G. Hu, X. Ma, *ACS Appl. Mater. Interfaces* **2019**, *11*, 14399 – 14407; d) D. Ley, C. X. Guzman, K. H. Adolfsson, A. M. Scott, A. B. Braunschweig, *J. Am. Chem. Soc.* **2014**, *136*, 7809 – 7812; e) X. F. Wang, W. J. Guo, H. Xiao, Q. Z. Yang, B. Chen, Y. Z. Chen, C. H. Tung, L. Z. Wu, *Adv. Funct. Mater.* **2020**, *30*, 1907282; f) M. E. Shirbhate, S. Kwon, A. Song, S. Kim, D. Kim, H. Huang, Y. Kim, H. Lee, S. J. Kim, M. H. Baik, J. Yoon, K. M. Kim, *J. Am. Chem. Soc.* **2020**, *142*, 4975 – 4979; g) Z. Huang, X. Ma, *Cell Rep. Phys. Sci.* **2020**, *1*, 100167.

[3] a) N. Oya, T. Ikezaki, N. Yoshie, *Polym. J.* **2013**, *45*, 955 – 961; b) X. Z. Yan, D. H. Xu, J. Z. Chen, M. M. Zhang, B. J. Hu, Y. H. Yu, F. H. Huang, *Polym. Chem.* **2013**, *4*, 3312 – 3322; c) M. N. He, X. S. Chen, D. H. Liu, D. C. Wei, *Chin. Chem. Lett.* **2019**, *30*, 961 – 965; d) T. Zhang, X. Ma, H. Tian, *Chem. Sci.* **2020**, *11*, 482 – 487; e) J. Boekhoven, W. E. Hendriksen, G. J. Koper, R. Eelkema, J. H. van Esch, *Science* **2015**, *349*, 1075 – 1079; f) H. Chen, X. Ma, S. Wu, H. Tian, *Angew. Chem. Int. Ed.* **2014**, *53*, 14149 – 14152; *Angew. Chem.* **2014**, *126*, 14373 – 14376.

[4] a) D. Komáromy, M. Tezcan, G. Schaeffer, I. Maric, S. Otto, *Angew. Chem. Int. Ed.* **2017**, *56*, 14658 – 14662; *Angew. Chem.* **2017**, *129*, 14850 – 14854; b) Y. Altay, M. Altay, S. Otto, *Chem. Eur. J.* **2018**, *24*, 11911 – 11915; c) I. Nyrkova, E. Moulin, J. J. Armao IV, M. Maaloum, B. Heinrich, M. Rawiso, F. Niess, J.-J. Cid, N. Jouault, E. Buhler, A. N. Semenov, N. Giuseppone, *ACS Nano* **2014**, *8*, 10111 – 10124; d) P. Nowak, M. Colomb-Delsuc, S. Otto, J. Li, *J. Am. Chem. Soc.* **2015**, *137*, 10965 – 10969; e) J. W. Sadownik, E. Mattia, P. Nowak, S. Otto, *Nat. Chem.* **2016**, *8*, 264 – 269.

[5] a) Y. Yan, J. Huang, B. Z. Tang, *Chem. Commun.* **2016**, *52*, 11870 – 11884; b) H. Choi, S. Heo, S. Lee, K. Y. Kim, J. H. Lim, S. H. Jung, S. S. Lee, H. Miyake, J. Y. Lee, J. H. Jung, *Chem. Sci.* **2020**, *11*, 721 – 730; c) J. S. Valera, R. Gomez, L. Sanchez, *Small* **2018**, *14*, 1702437; d) P. A. Korevaar, S. J. George, A. J. Markvoort, M. M. Smulders, P. A. Hilbers, A. P. Schenning, T. F. De Greef, E. W. Meijer, *Nature* **2012**, *481*, 492 – 496; e) A. T. Haedler, S. C. Meskers, R. H. Zha, M. Kivala, H. W. Schmidt, E. W. Meijer, *J. Am. Chem. Soc.* **2016**, *138*, 10539 – 10545; f) Y. Guo, Y. Liu, Y. Gong, W. Xiong, C. Zhang, J. Zhao, Y. Che, *Chem. Eur. J.* **2019**, *25*, 7463 – 7468; g) M. Endo, T. Fukui, S. H. Jung, S. Yagai, M. Takeuchi, K. Sugiyasu, *J. Am. Chem. Soc.* **2016**, *138*, 14347 – 14353; h) G. Ben Messaoud, P. Le Griel, D. Hermida-Merino, S. L. K. W. Roelants, W. Soetaert, C. V. Stevens, N. Baccile, *Chem. Mater.* **2019**, *31*, 4817 – 4830.

[6] a) K. Hu, Y. Liu, W. Xiong, Y. J. Gong, Y. K. Che, J. C. Zhao, *Chem. Mater.* **2019**, *31*, 1403 – 1407; b) M. Wehner, M. I. S. Rohr, M. Buhler, V. Stepanenko, W. Wagner, F. Würthner, *J. Am. Chem. Soc.* **2019**, *141*, 6092 – 6107; c) X. Ma, Y. Zhang, Y. Zhang, Y. Liu, Y. Che, J. Zhao, *Angew. Chem. Int. Ed.* **2016**, *55*, 9539 – 9543; *Angew. Chem.* **2016**, *128*, 9691 – 9695; d) B. Kemper, L. Zengerling, D. Spitzer, R. Otter, T. Bauer, P. Besenius, *J. Am. Chem. Soc.* **2018**, *140*, 534 – 537; e) T. Fukui, S. Kawai, S. Fujinuma, Y. Matsushita, T. Yasuda, T. Sakurai, S. Seki, M. Takeuchi, K. Sugiyasu, *Nat. Chem.* **2017**, *9*, 493 – 499.

[7] a) J. R. Gong, S. B. Lei, G. B. Pan, L. J. Wan, Q. H. Fan, C. L. Bai, *Colloids Surf.* **2005**, *257 – 258*, 9 – 13; b) X. Chi, H. Zhang, G. I. Vargas-Zuniga, G. M. Peters, J. L. Sessler, *J. Am. Chem. Soc.* **2016**, *138*, 5829 – 5832; c) D. Zhao, T. van Leeuwen, J. Cheng, B. L. Feringa, *Nat. Chem.* **2017**, *9*, 250 – 256; d) T. van Leeuwen, A. S. Lubbe, P. Štacko, S. J. Wezenberg, B. L. Feringa, *Nat. Rev. Chem.* **2017**, *1*, 0096.

[8] a) Z. Zhang, Y. S. Wu, K. C. Tang, C. L. Chen, J. W. Ho, J. Su, H. Tian, P. T. Chou, *J. Am. Chem. Soc.* **2015**, *137*, 8509 – 8520; b) W. Chen, C. L. Chen, Z. Zhang, Y. A. Chen, W. C. Chao, J. Su, H. Tian, P. T. Chou, *J. Am. Chem. Soc.* **2017**, *139*, 1636 – 1644; c) Z. Zhang, G. Sun, W. Chen, J. Su, H. Tian, *Chem. Sci.* **2020**, *11*, 7525 – 7537.

[9] a) H. Zhang, X. Zheng, R. T. K. Kwok, J. Wang, N. L. C. Leung, L. Shi, J. Z. Sun, Z. Tang, J. W. Y. Lam, A. Qin, B. Z. Tang, *Nat. Commun.* **2018**, *9*, 4961; b) A. H. G. David, R. Casares, J. M. Cuerva, A. G. Campana, V. Blanco, *J. Am. Chem. Soc.* **2019**, *141*, 18064 – 18074; c) Y. Sheng, D. Shen, W. Zhang, H. Zhang, C. Zhu, Y. Cheng, *Chem. Eur. J.* **2015**, *21*, 13196 – 13200; d) G. Liu,

C. Zhou, W. L. Teo, C. Qian, Y. Zhao, *Angew. Chem. Int. Ed.* **2019**, *58*, 9366 – 9372; *Angew. Chem.* **2019**, *131*, 9466 – 9472.
[10] Y. Lin, M. Penna, M. R. Thomas, J. P. Wojciechowski, V. Leonardo, Y. Wang, E. T. Pashuck, I. Yarovsky, M. M. Stevens, *ACS Nano* **2019**, *13*, 1900 – 1909.
[11] a) A. Aliprandi, M. Mauro, L. De Cola, *Nat. Chem.* **2016**, *8*, 10 – 15; b) X. Zhang, J. Yin, J. Yoon, *Chem. Rev.* **2014**, *114*, 4918 – 4959.
[12] a) K. Ma, W. Chen, T. Jiao, X. Jin, Y. Sang, D. Yang, J. Zhou, M. Liu, P. Duan, *Chem. Sci.* **2019**, *10*, 6821 – 6827; b) Y. Sang, D. Yang, Z. Shen, P. Duan, M. Liu, *J. Phys. Chem. C* **2020**, *124*, 17274 – 17281; c) Y. Shi, P. Sang, G. Yin, R. Gao, X. Liang, R. Brzozowski, T. Odom, P. Eswara, Y. Zheng, X. Li, J. Cai, *Adv. Opt. Mater.* **2020**, *8*, 1902122.

Manuscript received: August 27, 2020
Accepted manuscript online: October 24, 2020
Version of record online: December 9, 2020

